Hindawi Publishing Corporation
International Journal of Photoenergy
Volume 2014, Article ID 642819, 12 pages
http://dx.doi.org/10.1155/2014/642819

Research Article

Effects of Nonuniform Incident Illumination on the Thermal Performance of a Concentrating Triple Junction Solar Cell

Fahad Al-Amri[1] and Tapas Kumar Mallick[2]

[1] *College of Technology, P.O. Box 7650, Dammam 31472, Saudi Arabia*
[2] *Environment & Sustainability Institute, University of Exeter, Penryn Campus, Cornwall TR10 9EZ, UK*

Correspondence should be addressed to Fahad Al-Amri; alamrifahad@hotmail.com

Received 24 February 2014; Revised 20 May 2014; Accepted 21 May 2014; Published 16 June 2014

Academic Editor: Mark van Der Auweraer

A numerical heat transfer model was developed to investigate the temperature of a triple junction solar cell and the thermal characteristics of the airflow in a channel behind the solar cell assembly using nonuniform incident illumination. The effects of nonuniformity parameters, emissivity of the two channel walls, and Reynolds number were studied. The maximum solar cell temperature sharply increased in the presence of nonuniform light profiles, causing a drastic reduction in overall efficiency. This resulted in two possible solutions for solar cells to operate in optimum efficiency level: (i) adding new receiver plate with higher surface area or (ii) using forced cooling techniques to reduce the solar cell temperature. Thus, surface radiation exchanges inside the duct and Re significantly reduced the maximum solar cell temperature, but a conventional plain channel cooling system was inefficient for cooling the solar cell at medium concentrations when the system was subjected to a nonuniform light distribution. Nonuniformity of the incident light and surface radiation in the duct had negligible effects on the collected thermal energy.

1. Introduction

Nonuniformity of the incident illumination in concentrated photovoltaic (CPV) systems occurs as a result of using concentrating optics that reflect or refract light flux on the solar cell surface. The optimal optical system design would concentrate radiation on the solar cell surface in a uniform distribution. However, existing concentrators condense the majority of the incident flux onto a limited area of the cell surface, and most areas of the cell receive the remaining small amount of radiation. This situation produces a highly nonuniform irradiance distribution on the photovoltaic cells. This nonuniformity has two main effects on the solar cell: (i) electrical impacts, such as high ohmic drops and the flow of an internal current, and (ii) thermal impacts, such as increased temperatures in some regions of the cell that cause hot spots and drastically reduce the overall efficiency and power output. This reduction of power limits the viability of photovoltaic cells as an alternative energy source.

Previous studies reported thermal behavior of the CPV solar cells, such as Min et al. [1] and Cotal and Frost [2] who developed a theoretical thermal model for predicting the temperature of a multijunction solar cell based on passive cooling systems. Vincenzi et al. [3] used a silicon wafer with microchannels circulating water directly beneath the cells as an active cooling system. Moshfegh and Sandberg [4] performed both a numerical study and an experimental study of the flow and heat transfer characteristics of natural air convection behind solar cells. The results demonstrated that surface radiation significantly affects the temperature and conversion efficiency of the solar panel. Bhargava et al. [5], Garg and Adhikari [6], and Hegazy [7] analyzed the performance of hybrid photovoltaic/thermal (PV/T) air heating collectors and reported the effects of different design and controlling parameters on system performance. Al-Amri and Mallick [8, 9] recently developed a numerical heat transfer model for predicting the maximum cell temperatures of multijunction concentrating solar cell systems that were actively cooled by water-forced and air-forced convection. The maximum cell temperature was strongly dependent on the inlet velocity and the channel width. Teo et al. [10] experimentally investigated an active cooling system for

photovoltaic modules. A parallel array of ducts with an inlet/outlet manifold was attached to the back of the PV panel. When an air-based active cooling mechanism was employed, the temperature dropped effectively, leading to a 12% to 14% increase in the efficiency of the solar cells. Kumar et al. [11] presented a numerical heat transfer model for a novel concentrating photovoltaic design for the active solar panel initiative system (ASPIS). The incorporation of microchannels is an innovative way to remove a large amount of heat from a small cell surface that is associated with a high concentration [12, 13]. Tuckerman and Pease [14] pioneered the use of the microchannel heat sink for cooling planar integrated circuits. Several additional studies [15–17] were performed to analyze the heat transfer performance and the pressure drop of flows in microchannels. Qu and Mudawar [18] investigated the pressure drop and heat transfer performance of a laminar flow in a microchannel both experimentally and numerically. The microchannel was 213 μm wide and 713 μm deep. The results of this study indicated that the flow in this system is still governed by conventional equations for the conservation of mass, momentum, and energy. Micheli et al. [19] recently presented an overview of micro- and nanotechnologies that are applicable to passive CPV cooling and associated manufacturing technologies (e.g., monolithic applications). The authors reported that carbon nanotubes and high-conductive coating are the technologies that offer the best CPV cooling performance. This technological review was also critically assessed.

The problem of nonuniform illumination patterns has been studied extensively. However, most of these studies focused on the effects of nonuniformity on electrical performance [12]. Few studies investigated the thermal impacts of nonuniformity in radiation profiles. Franklin and Conventry [20] demonstrated both numerically and experimentally that a silicon solar cell under nonuniform focused illumination experiences a drop in both open-circuit voltage and efficiency compared to a cell under uniform illumination. In addition, the results indicated that the temperature profile closely resembles a Gaussian distribution. Coventry et al. [21] measured the thermal and electrical output from a concentrating PV/thermal collector at 25–30 suns. While the overall concentration ratio was approximately 30x, the illumination flux intensity across the width of the solar cell was far from even. Domenech-Garret [22] investigated the effects of a combination of nonuniform illumination and nonuniform temperature on a silicon solar cell. He used Gaussian and inverse Gaussian profiles to describe the temperature in the cell, which simulated a general cell cooling device. Chemisana and Rosell [23] studied the effects of Gaussian and anti-Gaussian temperature profiles on the cell's electrical parameters under different types of concentrated illumination both numerically and experimentally. The electric conversion efficiency increases under a Gaussian temperature profile and decreases when the cell is subjected to an inverse Gaussian temperature curve. The authors concluded that the temperature profile could be tailored to maximize efficiency for determined radiation conditions.

The studies presented above failed to adequately address the effects of nonuniformity of the incident flux on the temperature profiles of CPV systems. Thus, further studies of heat transfer characteristics under nonuniform flux are necessary to understand the effect of this nonuniformity on the overall efficiency of the solar cell. The objective of this investigation was to extend the work of Al-Amri and Mallick [8] by assessing the effect of nonuniform incident light on the temperature distribution of a concentrated triple junction solar cell.

A heat transfer model was developed to simulate the temperature distribution on the concentrated solar cells under a nonuniform incident light. The results of this study are important for determining the overall efficiency of a CPV system and for promoting the development of a cooling system and new concentrators.

2. Mathematical Formulations

The geometry of the physical problem and the coordinate system considered in this study are presented in Figure 1. The components consist of a triple junction GaInP/GaAs/Ge solar cell, a Cu-Ag-Hg front contact to the solar cell, a 2 mm glass cover, a 1.5 mm thick aluminum back plate, and a 0.5 mm adhesive material used to attach the solar cell to the cover glass and the rear aluminum plate. The cooling air is forced to flow within the ducts behind the back plate, whose external wall is assumed to be adiabatic. The two walls of the duct are assumed to be gray, opaque, and diffuse surfaces. The inlet and exit channel areas are assumed to be black at the ambient temperature ($T_\infty = 27^\circ$C) and the exit bulk temperature (T_e), respectively. The efficiency of the triple junction solar cell (η) is 0.38 and the reflectivity is assumed to be zero for all solar cell components except for the front contact metal which is assumed to be 0.85. Table 1 shows the dimensions and the thermophysical properties of the components used in the model.

The illumination distribution incident on the cell surface in a concentrator system consisting of reflective troughs is highly non-uniform and takes the shape of a Gaussian profile [12]. Thus, the illumination intensity formula adopted in the current model is

$$I(z) = \frac{2C}{10^4 \mathrm{SD}\sqrt{2\pi}} e^{-(2(z-z_0)^2)/\mathrm{SD}^2}, \quad (1)$$

where z_0 is the position of the maximum illumination on the cell surface and SD is the standard deviation, which measures how far incident illumination is spread out.

The intensity of incident light $I(z)$ can be written in the nondimensional form as follows:

$$\bar{I}(Z) = \frac{I(z)}{I_{\mathrm{avg}}}, \quad (2)$$

where I_{avg} is the average incident illumination across the entire cell surface.

The physical problem depicted in Figure 1 is governed by equations of energy conservation in both the multiwalls (solar cell assembly) and the fluid inside the duct and by equations of continuity, momentum in the fluid region, and radiation constraint along each of the two duct surfaces as

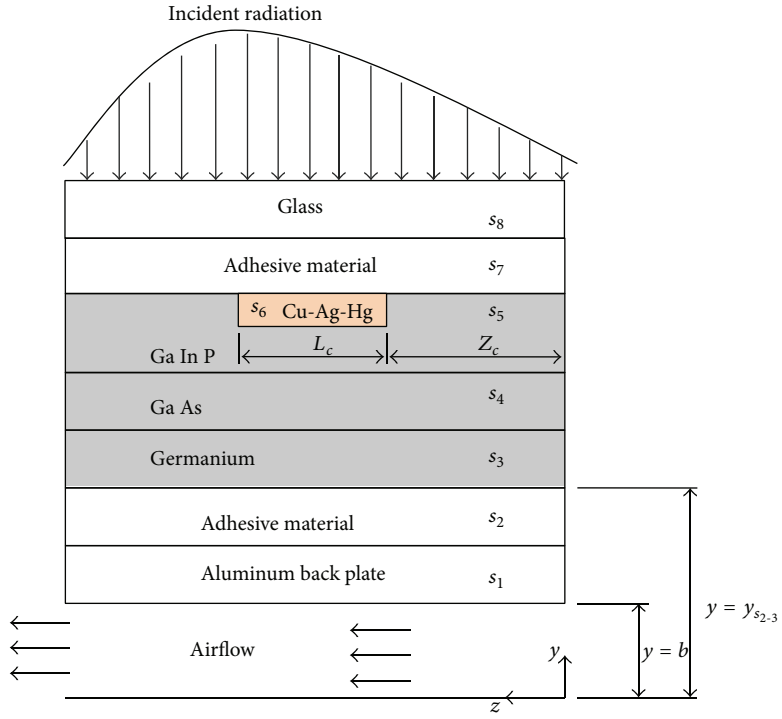

Figure 1: Schematic of the geometry of the employed system.

Table 1: Thermophysical properties assumed in the simulation.

Component	Material	Length (mm)	Thickness (mm)	Thermal conductivity W/m·K	Absorptivity
Solar cell	GuInp	10	0.1	73	0.04
	GuAs	10	0.2	65	0.40
	Ge	10	0.2	60	0.50
Front contact	Cu + Ag + Hg	2	0.025	300	0.15
Glass cover	Low-iron glass	10	2	12	0.04
Adhesive		10	0.5	50	0.02
Back plate	Aluminium	10	1.5	238	

a result of surface radiation exchange between the two walls of the channel. Using typical boundary layer assumptions and neglecting the axial conduction of heat in both the solid and the fluid regions, the corresponding equations governing the conjugate laminar mixed flow and the heat transfer in the entry region of the two parallel plates can be expressed in the following dimensionless forms.

Continuity Equation. Consider

$$\frac{\partial V}{\partial Y} + \frac{\partial U}{\partial Z} = 0. \tag{3}$$

Momentum Equation. Consider

$$V\frac{\partial U}{\partial Y} + U\frac{\partial U}{\partial Z} = -\frac{dP}{dZ} + \frac{G_r^*}{\mathrm{Re}}\left(\theta - \theta_\infty\right) + \frac{\partial^2 U}{\partial Y^2}. \tag{4}$$

Energy Equation for the Fluid. Consider

$$V\frac{\partial \theta_f}{\partial Y} + U\frac{\partial \theta_f}{\partial Z} = \frac{1}{\mathrm{Pr}}\frac{\partial^2 \theta_f}{\partial Y^2}. \tag{5}$$

Energy Equation for Each Solid Material in Solar Cell Assembly. Consider

$$\frac{\partial^2 \theta_s}{\partial Y^2} = 0. \tag{6}$$

The integral form of the continuity equation (1) can be written in the following form [24]:

$$F = \int_0^1 U dY = 1. \tag{7}$$

The radiation constraint equations can be derived by applying the first law of thermodynamic per unit area of the surface on

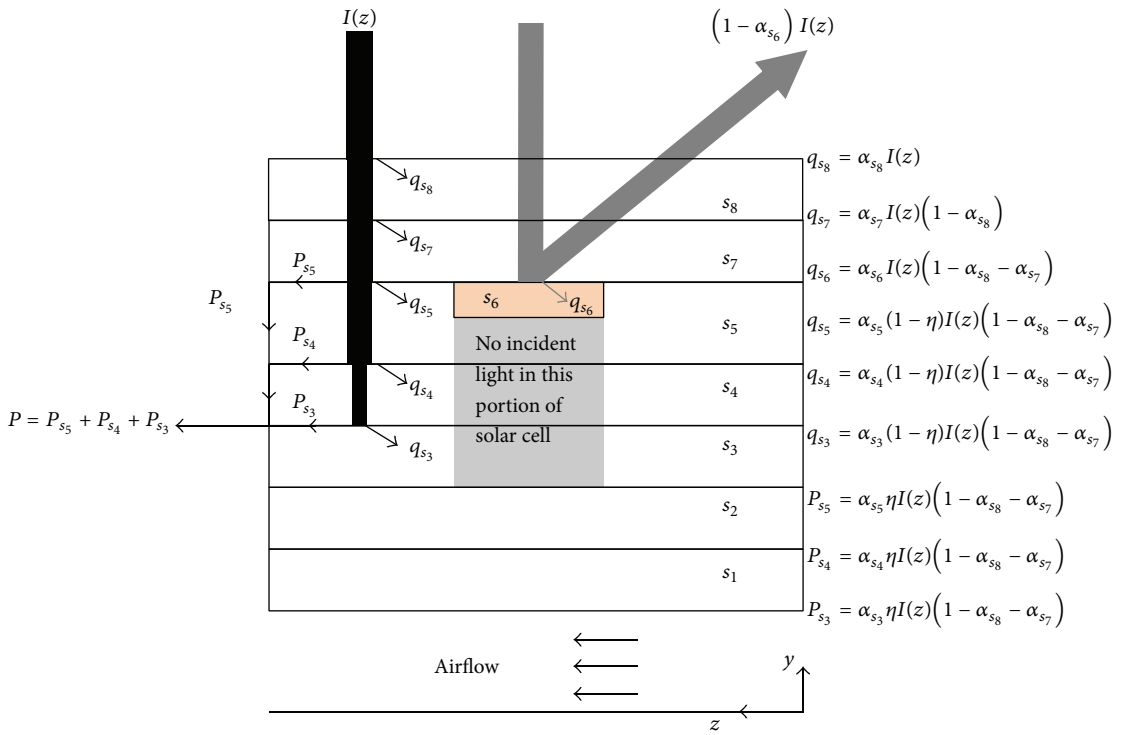

Figure 2: Energy fluxes in solar cell assembly.

the channel plate element [25] which yields the following two equations.

Surface 1 ($Y = 0$). Consider

$$\begin{aligned}
&N_{\text{rad}}\theta_{\infty}^{4}\left[\frac{1}{2}-\left(\frac{Z\,\text{Re}}{2}\right)\left(1+Z^{2}\text{Re}^{2}\right)^{-1/2}\right]\\
&\quad+N_{\text{rad}}\theta_{e}^{4}\left[\frac{1}{2}-\left(\frac{(L-Z)\,\text{Re}}{2}\right)\left(1+(L-Z)^{2}\text{Re}^{2}\right)^{-1/2}\right]\\
&\quad+\int_{0}^{L}\left\{\frac{1-\varepsilon_{2}}{\varepsilon_{2}}\left(\left.\frac{\partial\theta_{f}}{\partial Y}\right|_{Y=1^{-}}-\left.\frac{\partial\theta_{s}}{\partial Y}\right|_{Y=1^{+}}\right)+N_{\text{rad}}\theta_{w2}^{4}(Z)\right\}\\
&\quad*\frac{1}{2}\left[1+\text{Re}^{2}\left(Z-Z'\right)^{2}\right]^{(-3/2)}\text{Re}\,dZ'\\
&=\frac{1-\varepsilon_{1}}{\varepsilon_{1}}\left[-\left.\frac{\partial\theta_{f}}{\partial Y}\right|_{Y=0^{+}}\right]\\
&\quad+N_{\text{rad}}\theta_{w_1}^{4}(Z)-\left.\frac{\partial\theta_{f}}{\partial Y}\right|_{Y=0^{+}}
\end{aligned}$$

$$\text{Where: } N_{\text{rad}}=\sigma q_{\text{avg}}^{3}\frac{b^{4}}{k_{f}^{4}}. \tag{8}$$

Surface 2 ($Y = 1$). Consider

$$\begin{aligned}
&\text{KR}_{s_1-f}\left.\frac{\partial\theta_{s}}{\partial Y}\right|_{Y=1^{+}}+N_{\text{rad}}\theta_{\infty}^{4}\left[\frac{1}{2}-\left(\frac{Z\,\text{Re}}{2}\right)\right.\\
&\qquad\left.\times\left(1+Z^{2}\text{Re}^{2}\right)^{-1/2}\right]\\
&\quad+N_{\text{rad}}\theta_{e}^{4}\left[\frac{1}{2}-\left(\frac{(L-Z)}{2}\,\text{Re}\right)\right.\\
&\qquad\left.\times\left(1+(L-Z)^{2}\text{Re}^{2}\right)^{-1/2}\right]\\
&\quad+\int_{0}^{L}\left\{\frac{1-\varepsilon_{1}}{\varepsilon_{1}}\left(-\left.\frac{\partial\theta}{\partial Y}\right|_{Y=0^{+}}\right)+N_{\text{rad}}\theta_{w1}^{4}(Z)\right\}\\
&\quad*\frac{1}{2}\left[1+\text{Re}^{2}\left(Z-Z'\right)^{2}\right]^{(-3/2)}\text{Re}\,dZ'\\
&=\frac{1-\varepsilon_{2}}{\varepsilon_{2}}\left[\left.\frac{\partial\theta_{f}}{\partial Y}\right|_{Y=1^{-}}-\left.\frac{\partial\theta_{s}}{\partial Y}\right|_{Y=1^{+}}\right]\\
&\quad+N_{\text{rad}}\theta_{w_2}^{4}(Z)-\left.\frac{\partial\theta_{f}}{\partial Y}\right|_{Y=1^{-}}.
\end{aligned} \tag{9}$$

When surface radiation is absent (i.e., $\varepsilon = 0$), (7) and (8) are reduced to

$$\begin{aligned}
\left.\frac{\partial\theta_{f}}{\partial Y}\right|_{Y=0}&=0,\\
\text{KR}_{s_1-f}\left.\frac{\partial\theta_{s}}{\partial Y}\right|_{Y=1^{+}}&=\left.\frac{\partial\theta_{f}}{\partial Y}\right|_{Y=1^{-}}.
\end{aligned} \tag{10}$$

The conjugate convection field equations are subject to the following dimensionless boundary conditions.

In the Fluid Region. For $Z = 0$ and $0 < Y < 1$,

$$U=1,\qquad V=P=0,\qquad \theta=\theta_{\infty}. \tag{11a}$$

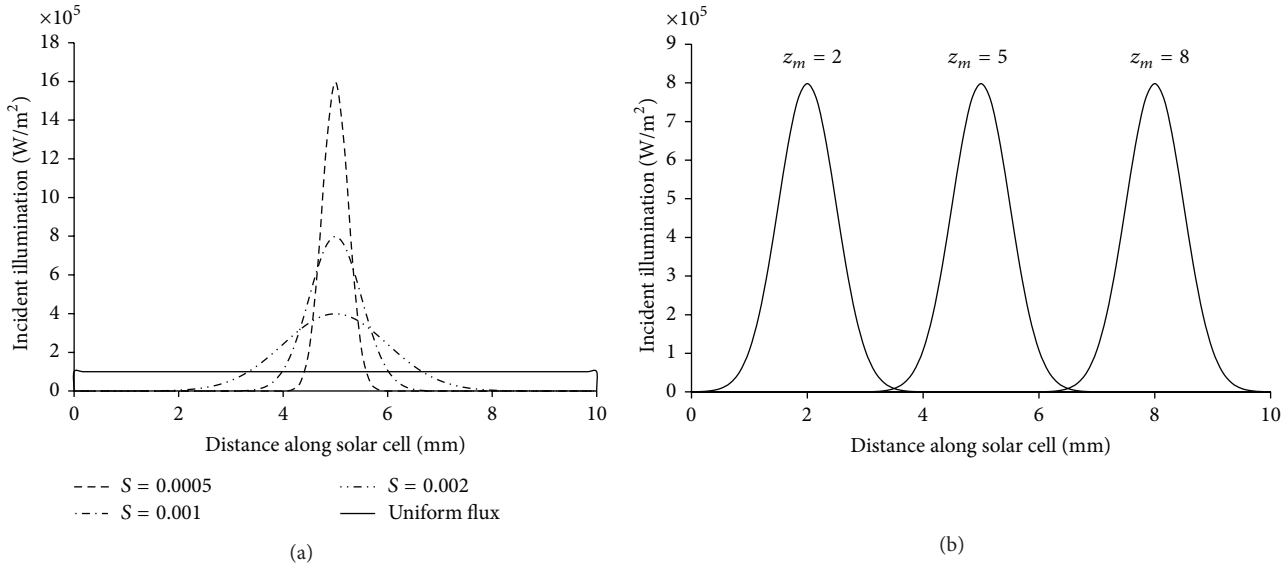

Figure 3: Incident illumination profiles for $C = 100$ at (a) different values of SD and (b) different values of z_0.

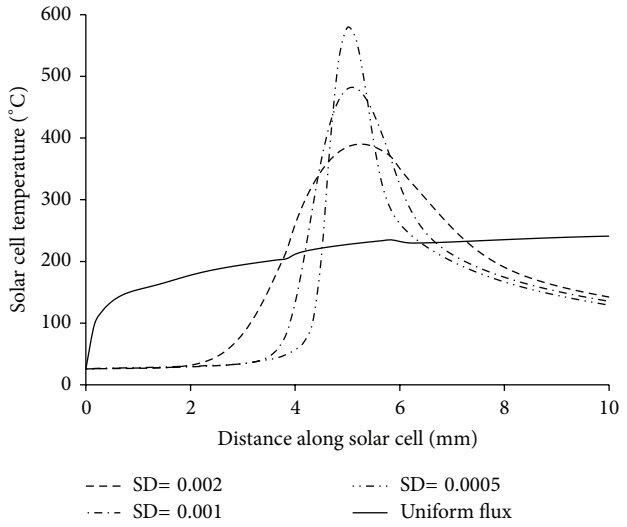

Figure 4: Variations in solar cell temperature obtained using different values of SD, when $z_0 = 0.5$, Re = 500, $\varepsilon = 0.95$, and $C = 100$.

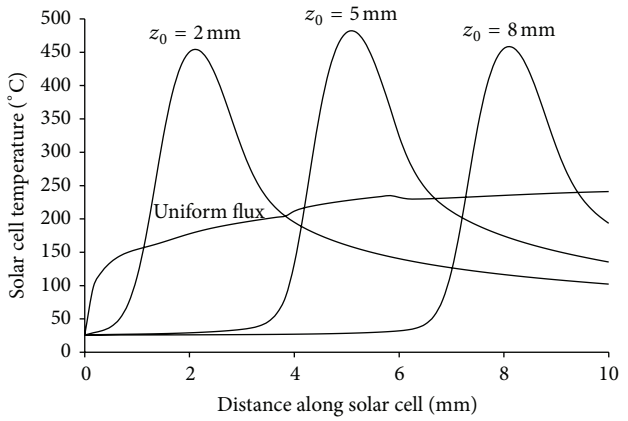

Figure 5: Variations in solar cell temperature obtained using different values of z_0, when SD = 0.001, Re = 500, $\varepsilon = 0.95$, and $C = 100$.

For $Z > 0$ and $Y = 0$,

$$U = V = 0. \tag{11b}$$

For $Z > 0$ and $Y = 1$,

$$U = V = 0. \tag{11c}$$

In the Solid Region (solar cell assembly). In the present model, we assumed that some of the incident light is absorbed by each surface of solar cell assembly layers based on the value of absorptivity and converted into thermal and/or electrical energy. Then, heat is diffused to the next layer by conduction. Each layer of the solar cell is in the order of 100 to 200 microns; therefore, the skin depth of each layer is assumed to be thin and the radiation effects are confined to the surface layer. The boundary conditions in this region can be deduced by applying the continuity of temperature and heat flux at the solid-solid interface. Taking a surface energy balance at each solid-solid interface (see Figure 2) leads to the following boundary condition equations.

For $Z > 0$ and $Y = Y_{s_{(i)-(i+1)}}$, $i = 1$ and 2,

$$\left.\frac{\partial \theta_s}{\partial Y}\right|_{Y=Y^-_{s_{(i)-(i+1)}}} = \mathrm{KR}_{s_{(i+1)-(i)}} \left.\frac{\partial \theta_s}{\partial Y}\right|_{Y=Y^+_{s_{(i)-(i+1)}}}. \tag{11d}$$

For $Y = Y_{s_{(i)-(i+1)}}$ and $0 < Z < Z_c$ or $(Z_c + L_c) < Z < L$, $i = 3$ and 4,

$$\left.\frac{\partial \theta_s}{\partial Y}\right|_{Y=Y^-_{s_{(i)-(i+1)}}} = \mathrm{kR}_{s_{(i+1)-(i)}} \left.\frac{\partial \theta_s}{\partial Y}\right|_{Y=Y^+_{s_{(i)-(i+1)}}} + \frac{(1-\eta)\,\alpha_{s_i}\left(1-\alpha_{s_8}-\alpha_{s_7}\right)\overline{I}\,(Z)}{\mathrm{KR}_{s_i-f}}. \tag{11e}$$

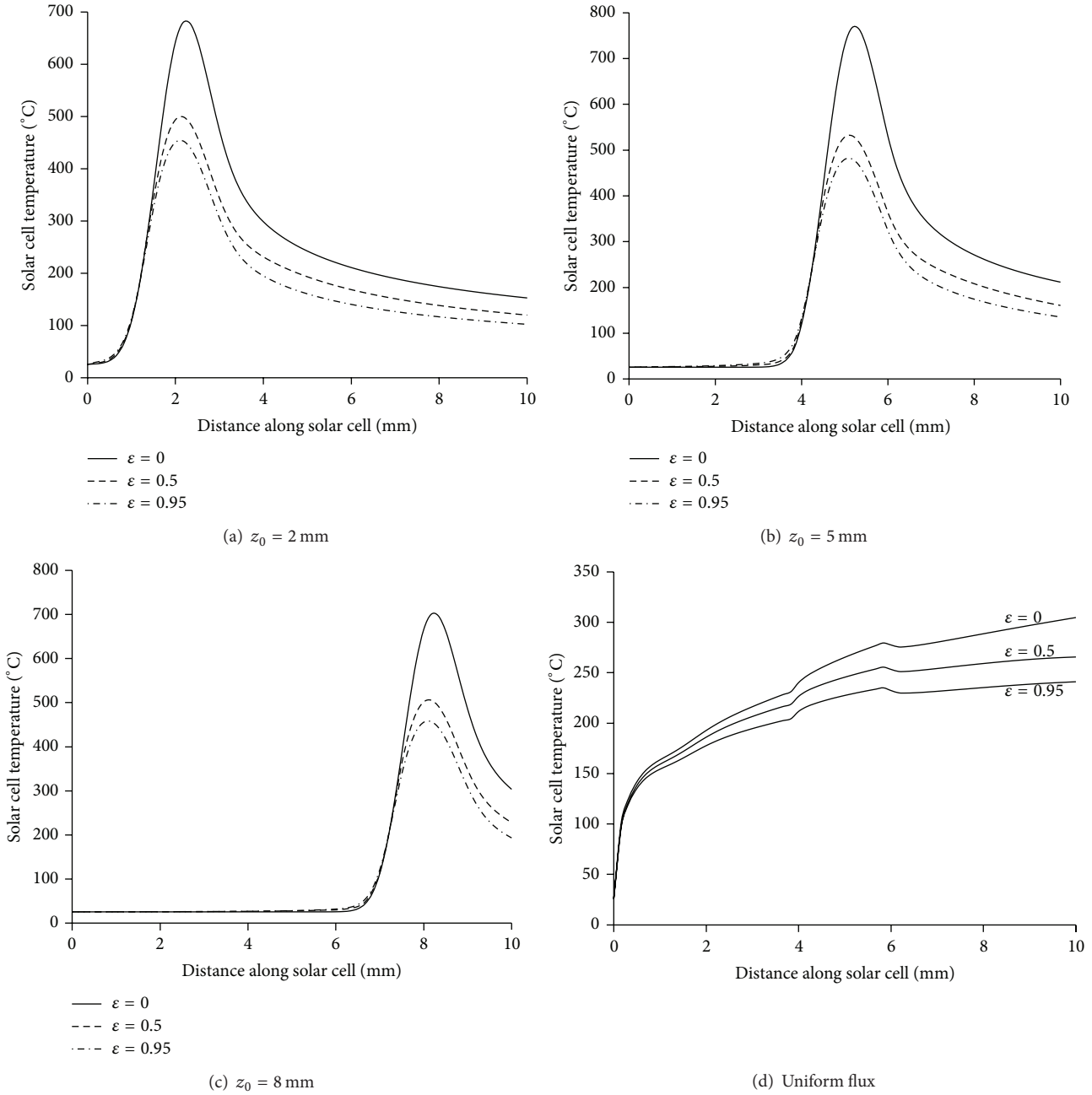

Figure 6: Variations in solar cell temperature obtained using different values of ε, when SD = 0.001, Re = 500, and C = 100.

For $Y = Y_{s_{5-7}}$ and $0 < Z < Z_c$ or $(Z_c + L_c) < Z < L$,

$$\left.\frac{\partial\theta_s}{\partial Y}\right|_{Y=Y^-_{s_{5-7}}} = \mathrm{kR}_{s_{7-5}} \left.\frac{\partial\theta_s}{\partial Y}\right|_{Y=Y^+_{s_{5-7}}} + \frac{(1-\eta)\,\alpha_{s_5}\left(1-\alpha_{s_8}-\alpha_{s_7}\right)\overline{I}\,(Z)}{\mathrm{KR}_{s_5-f}}. \tag{11f}$$

For $Y = Y_{s_{(i)-(i+1)}}$ and $Z_c \le Z \le (Z_c + L_c)$, i = 3, 4, and 5,

$$\left.\frac{\partial\theta}{\partial Y}\right|_{Y=Y^-_{s_{(i)-(i+1)}}} = \mathrm{kR}_{s_{(i+1)-(i)}} \left.\frac{\partial\theta}{\partial Y}\right|_{Y=Y^+_{s_{(i)-(i+1)}}}. \tag{11g}$$

For $Y = Y_{s_{6\text{-}7}}$ and $Z_c \le Z \le (Z_c + L_c)$,

$$\left.\frac{\partial\theta}{\partial Y}\right|_{Y=Y^-_{s_{6\text{-}7}}} = \mathrm{kR}_{s_{7\text{-}6}} \left.\frac{\partial\theta}{\partial Y}\right|_{Y=Y^+_{s_{6\text{-}7}}} + \frac{\alpha_{s_6}\left(1-\alpha_{s_8}-\alpha_{s_7}\right)\overline{I}\,(Z)}{\mathrm{kR}_{s_6-f}}. \tag{11h}$$

For $Z > 0$ and $Y = Y_{s_{7\text{-}8}}$,

$$\left.\frac{\partial\theta}{\partial Y}\right|_{Y=Y^-_{s_{7\text{-}8}}} = \mathrm{kR}_{s_{8\text{-}7}} \left.\frac{\partial\theta}{\partial Y}\right|_{Y=Y^+_{s_{7\text{-}8}}} + \frac{\alpha_{s_7}\left(1-\alpha_{s_8}\right)\overline{I}\,(Z)}{\mathrm{kR}_{s_7-f}}. \tag{11i}$$

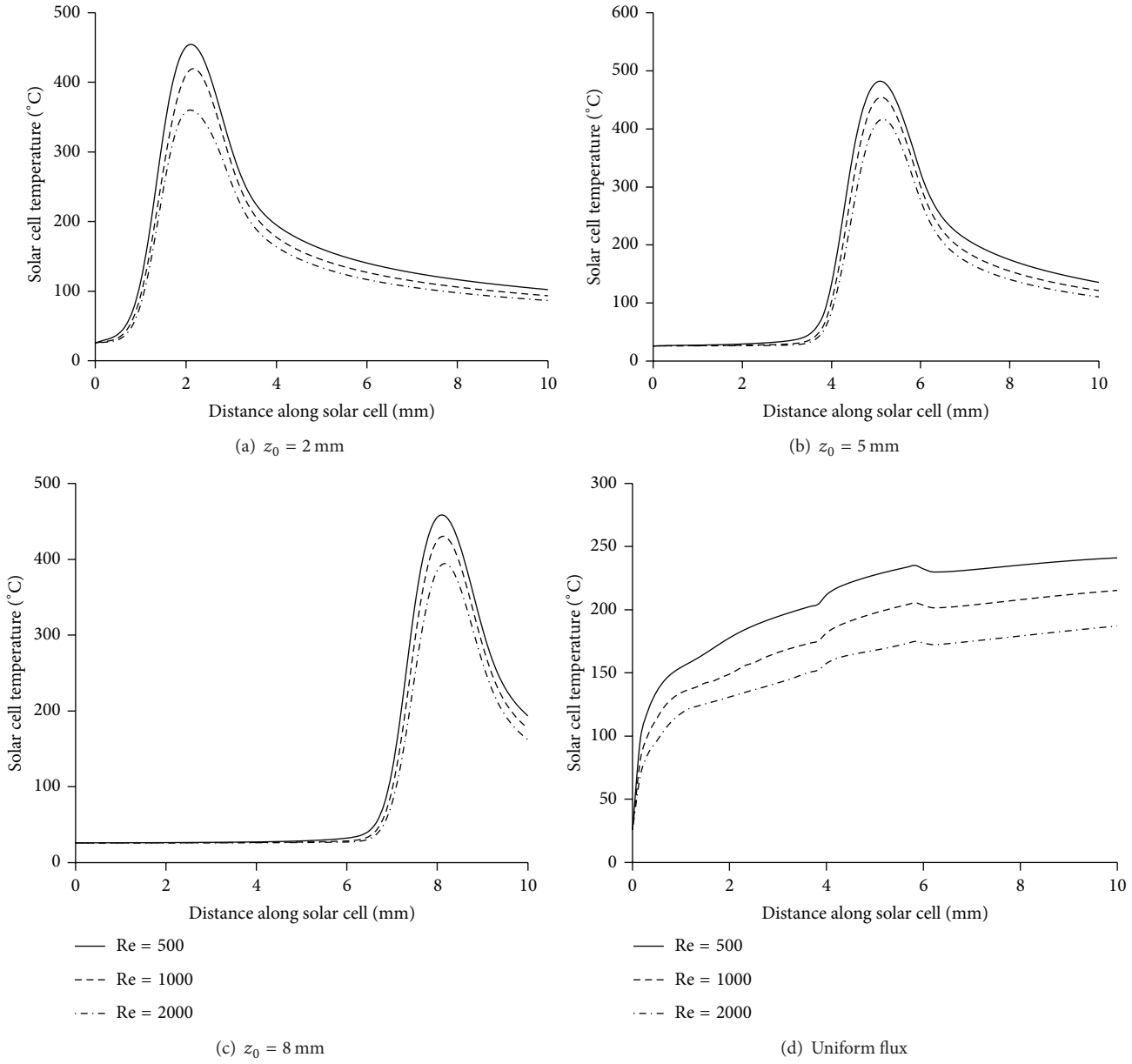

Figure 7: Variations in solar cell temperature obtained using different values of Re, when SD = 0.001, $\varepsilon = 0.95$, and $C = 100$.

For $Z > 0$ and $Y = Y_{s_8}$,

$$\left.\frac{\partial\theta}{\partial Y}\right|_{Y=Y_{s_8}} = \frac{\alpha_{s_8}\bar{I}(Z)}{\mathrm{kR}_{s_8-f}}, \tag{11j}$$

where $\mathrm{kR}_{s_{(i+1)-i}} = k_{s_{i+1}}/k_{s_i}$ and $\mathrm{kR}_{s_i-f} = k_{s_i}/k_f$.

3. Method of Solution

The conjugate convection field equations (i.e., continuity, momentum, and energy), the two radiation constraint equations, and the corresponding boundary conditions are transformed into finite difference equations. The conjugate convection field equations are initially solved using a numerical marching technique. The two radiation constraint equations are then solved iteratively to update the wall temperatures using the Gauss-Seidel technique. These updated wall temperatures are used to resolve the conjugate convection field equations. The process is then repeated until convergence is achieved. The details of the solution procedure and the validation of the numerical code can be found in Al-Amri and Mallick [9].

4. Results and Discussion

Figures 3(a) and 3(b) show the incident illumination profiles obtained using (1) for the concentration ratio $C = 100$ at three selected standard deviation values (SD = 0.0005, 0.001,

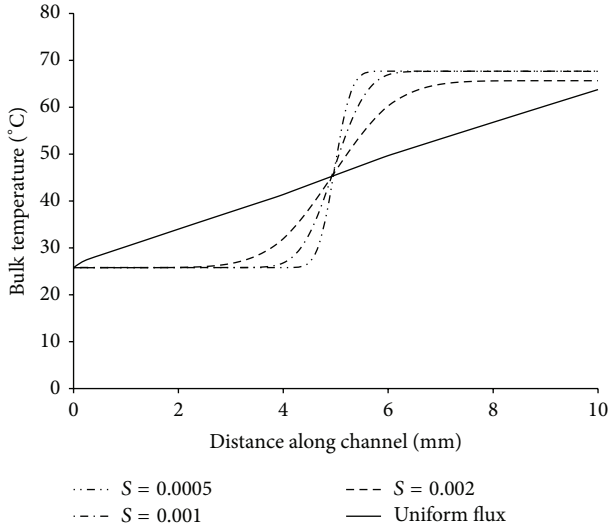

Figure 8: Variations in fluid bulk temperature obtained using different values of SD, when $z_m = 0.5$, Re = 500, $\varepsilon = 0.95$, and $C = 100$.

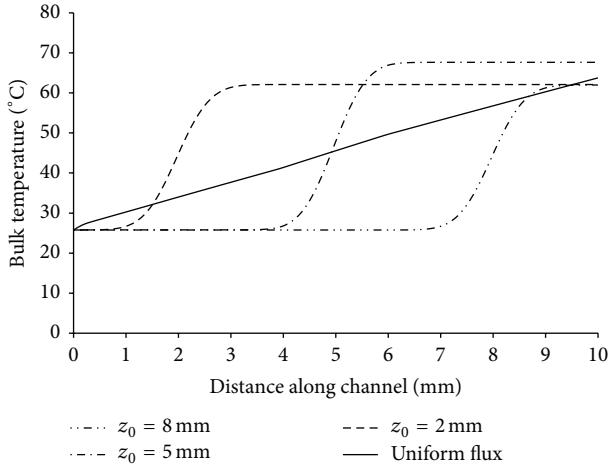

Figure 9: Variations in fluid bulk temperature obtained using different values of z_m, when SD = 0.001, Re = 500, $\varepsilon = 0.95$, and $C = 100$.

and 0.002) and three selected values for the position of the maximum illumination on the cell surface ($z_0 = 2, 5, 8$ mm), respectively. These profiles were used as input data in the code to study the effects of these parameters on the temperature distribution of the solar cell and the fluid bulk temperature. In addition, the effect of the emissivity of the two duct walls and the Reynolds number in the presence of nonuniform incident light was investigated.

4.1. Effect of a Nonuniform Light Profile on the Solar Cell Temperature. Figure 4 shows the variations of solar cell temperature with $z_0 = 5$ mm and with the axial distance from the channel entrance for both uniform and nonuniform incident light at SD = 0.0005, 0.001, and 0.002. For a uniform distribution, the results demonstrate that the solar cell temperature first increases sharply near the entrance and then gradually increases until reaching its maximum value at the channel exit. In addition, there is a sudden increase in cell temperature at $z = 4$ mm and a sudden decrease at $z = 6$ mm. These changes occur due to the fact that no current is generated in this portion of the solar cell and all of the light is converted to heat due to the presence of the Cu-Ag-Hg front contact. However, this increment is small (≈7°C) and has minor effects on the overall efficiency. For a nonuniform distribution, the temperature of the first quarter of the solar cell remains constant at ambient temperature, then rapidly increases, and reaches its maximum value at the center of the cell. The temperature then drops sharply and gradually in the fourth quarter of the solar cell where the temperatures are higher than those observed in the first quarter. The profile of the temperature becomes thinner and the maximum temperature increases as the SD decreases, as shown in Figure 4. In addition, the maximum temperature of the solar cell is much higher when using a nonuniform light distribution than when using a uniform light distribution. In this example, the maximum temperature obtained using a uniform light distribution was 240°C, which indicates that the solar cell can be operated with a reasonable efficiency as the modern multijunction solar cells can adequately be operated at this level of temperature [25, 26]. In contrast, the results obtained using a nonuniform light distribution indicate that the cell efficiency will be drastically reduced due to the high temperature of some portions of the cell surface.

The effects of the position of maximum incident light on the solar cell temperature distribution are shown in Figure 5. A hot spot formed on the portion of the cell surface that was exposed to a large amount of light. This hot spot is slightly hotter when $z_0 = 5$ mm (i.e., at the center of the solar cell) due to the presence of the front contact metal in this region. Figures 6(a)–6(d) show the effect of the emissivity of the two duct walls on the temperature profile of the solar cell for both uniform and nonuniform incident light when $z_0 = 2$, 5, and 8 mm and when $\varepsilon = 0$ (i.e., pure forced convection), 0.5, and 0.95. The results presented in these figures demonstrate that the maximum solar cell temperature decreases significantly as surface emissivity increases. However, the presence of surface radiation inside the channel does not change the shape of the temperature distribution for the nonuniform light profile. In this example, as emissivity increased from $\varepsilon = 0$ to 0.95, the maximum solar cell temperature was reduced by approximately 35% when using nonuniform illumination and 20% when using uniform illumination. The large contribution of surface radiation to the nonuniform light profile is due to the increase in the effective temperature differential for surface radiation between the two duct walls. Nevertheless, the maximum temperature of the solar cell when using nonuniform light was still higher than that obtained using a uniform light distribution. For the uniform light profile, surface radiation exchange between the two duct walls and between the heated duct wall and the inlet and exit areas of the channel leads to a reduction of maximum cell temperature from 305°C to 240°C, which enables the solar cell to operate with a reasonable efficiency.

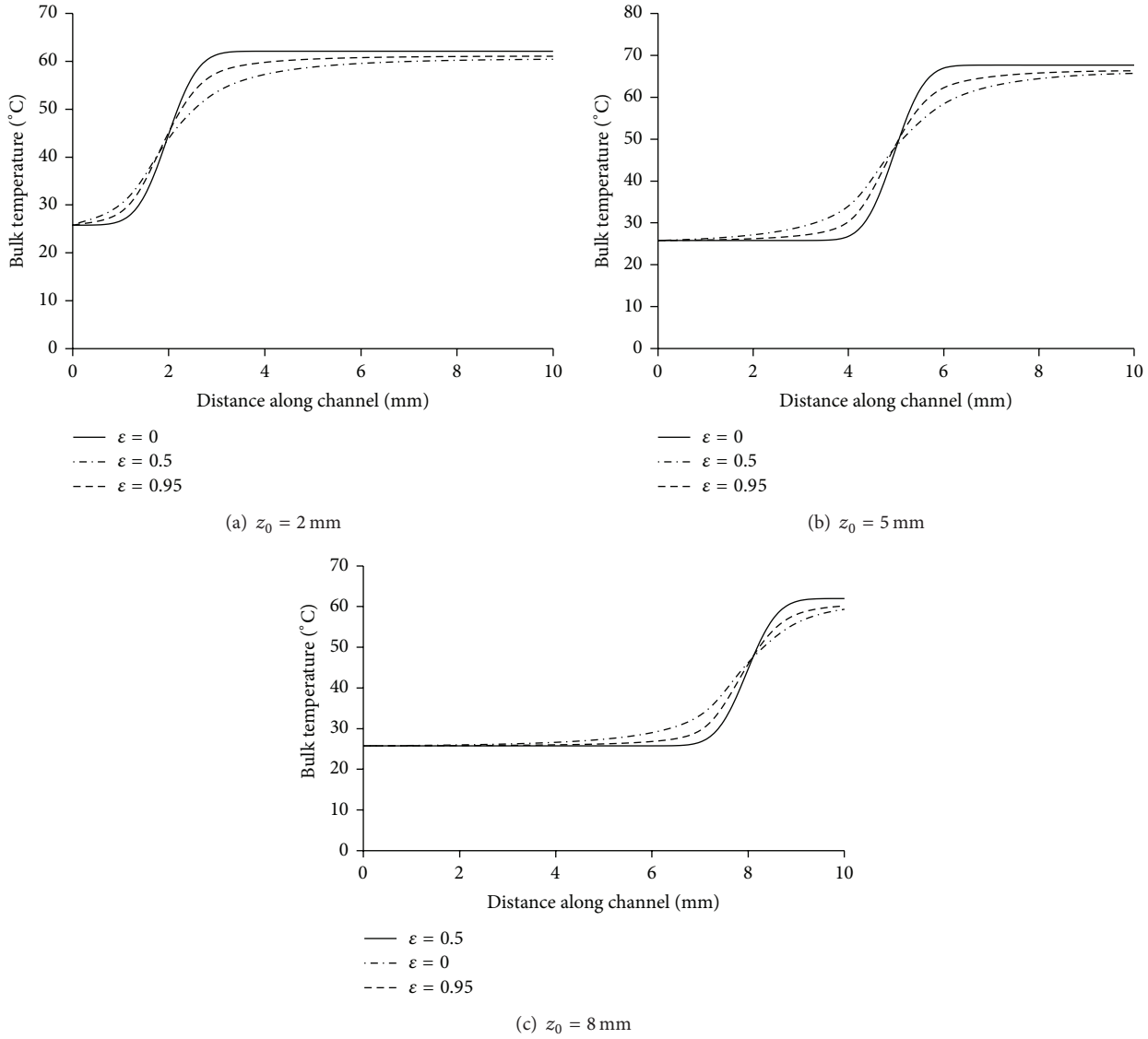

FIGURE 10: Variations in fluid bulk temperature obtained using different values of ε, when SD = 0.001, Re = 500, and C = 100.

The results presented in Figures 7(a)–7(c) illustrate the variations in solar cell temperature that occur with changes in axial distance from the channel entrance when using uniform and nonuniform light distributions, three selected values of Reynolds number (500, 1000, and 2000), and a given value of $\varepsilon = 0.95$. The cell temperature decreases with increasing Re, but the profile maintains its general shape. The percent reductions of maximum solar cell temperature that occurred as Reynolds number increased by 300% from 500 to 2000 were 20.7%, 13.4%, and 13.7% for $z_0 = 2$, 5, and 8 mm, respectively. This value was approximately 22.5% when a uniform light distribution was employed. These results indicate that, for nonuniform light profiles, increasing flow rate is more useful when the maximum incident light is located near the channel entrance because the difference between the wall temperature and the fluid temperature is high in this region, which enhances convective heat transfer.

4.2. Effect of a Nonuniform Light Profile on the Fluid Bulk Temperature. Figures 8 and 9 show the variation of fluid bulk temperature with increasing axial distance from the channel entrance under different incident light profiles. The results presented in these two figures demonstrate that the incident light distribution strongly influences the fluid bulk temperature profile inside the channel. However, the effect of the incident light profile on the fluid bulk temperature at the channel exit is insignificant. Figures 10(a), 10(b), and 10(c) show the effect of the emissivity of the two duct walls on the fluid bulk temperature when $z_0 = 2$, 5, and 8 mm, respectively. Surface radiation increased the temperature of the fluid closer to the entrance than pure convection (i.e., $\varepsilon = 0$) due to radiative heat exchanges between the heated and the adiabatic walls, which redistribute the temperature profiles of the walls and hence the convective heat transferred to the flowing fluid. The effect of emissivity on the fluid bulk

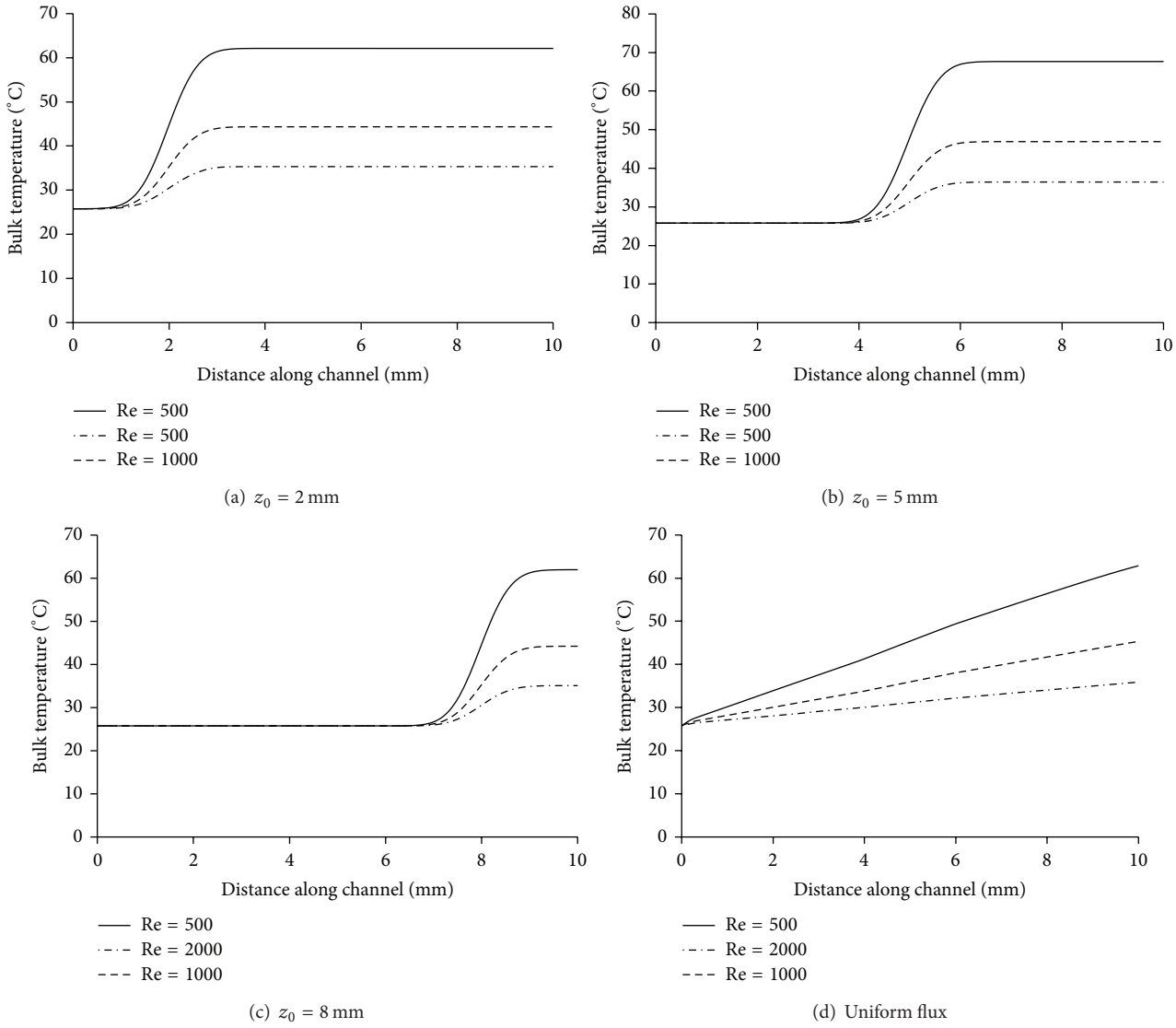

Figure 11: Variations in fluid bulk temperature obtained using different values of Re, when SD = 0.001, $\varepsilon = 0.95$, and $C = 100$.

temperature at the channel exit is insignificant, as shown in Figures 10(a)–10(c).

The effects of Re on the fluid bulk temperature are shown in Figures 11(a)–11(d) for uniform and nonuniform light flux. The results demonstrate that the fluid bulk temperature decreases with increasing Re. In this example, the fluid bulk temperature decreases by approximately 43% as Re increases by 300% for given values of controlling parameters. However, the collected thermal energy increases with increasing Re, as a result of increasing flow rate.

5. Conclusions

The effects of nonuniformity of the incident light on the temperature and fluid bulk temperature of a triple junction solar cell were studied. Nonuniformity was simulated using a Gaussian distribution. The results indicated that nonuniform illumination significantly alters the temperature distribution of the solar cell, causing hot spots in some regions of the solar cell. Although increasing the emissivity of the two duct walls and increasing Re can reduce the maximum solar cell temperature by as much as 35% and 20%, respectively, solar cell temperatures in the region exposed to the most incident light are high enough to cause degradation in solar cell efficiency at medium concentrations. Thus, secondary optical concentrators are required to redistribute the incident light on the cell surface into a uniform shape. Alternatively, an innovative cooling system, such as the introduction of a secondary jet flow into a channel, should be used to redistribute solar cell temperatures and reduce the maximum temperature to an acceptable value. Surface emissivity and nonuniform illumination affect the fluid bulk temperature distribution inside the channel. However, the effect of these parameters on fluid bulk temperature at the channel exit is insignificant.

Nomenclature

b: Channel width, m
C: Concentration ratio
Gr^*: Modified Grashof number, $g\beta q_{\mathrm{avg}} b^4/\upsilon^2 K_f$
I: Intensity of incident light, $\mathrm{W/m^2}$
k: Thermal conductivity, $\mathrm{W/m \cdot K}$
ℓ: Channel length, m
L: Dimensionless plate length, $= \ell/(b\ \mathrm{Re})$
p: Pressure of fluid at any cross section, $\mathrm{N/m^2}$
p': Pressure defect at any cross section, $p - p_s$, $\mathrm{N/m^2}$
p_s: Hydrostatic pressure, $-\rho_\infty g z$, $\mathrm{N/m^2}$
p_∞: Pressure of fluid at the channel entrance, $\mathrm{N/m^2}$
P: Dimensionless pressure at any cross section, $= (p' - p_\infty)/(\rho_\infty u_\infty^2)$
N_{rad}: Radiation number, $\sigma q_{\mathrm{avg}}^3 b^4/k_f^4$
q_{avg}: Average input heat flux, $= (1-\eta) I_{\mathrm{avg}}$, $\mathrm{W/m^2}$
Re: Reynolds number, $= u_o b/\upsilon$
t: Solar cell assembly thickness, m
T: Temperature at any point, K
T_∞: Inlet temperature, K
SD: Standard deviation
u_∞: Entrance axial velocity, m/s
u: Longitudinal velocity component at any point, m/s
U: Dimensionless longitudinal velocity, $U = u/u_\infty$
v: Transverse velocity component at any point, m/s
V: Dimensionless transverse velocity, $V = b * v/\upsilon$
y: Horizontal coordinate, m
Y: Dimensionless horizontal coordinate, y/b
z: Vertical coordinate, m
z_0: Position of the maximum incident light, m
Z: Dimensionless vertical coordinate, $z/(b * \mathrm{Re})$.

Greek Symbols

υ: Kinematic fluid viscosity
ρ: Fluid density, $\mathrm{kg/m^3}$
μ: Dynamic fluid viscosity, $\mathrm{kg}/m \cdot s$
α: Absorptivity
η: Efficiency of the solar cell
θ: Dimensionless temperature at any point $[=k_f T/q_{\mathrm{avg}} b]$
θ_∞: Dimensionless inlet temperature at any point $[=k_f T_\infty/q_{\mathrm{avg}} b]$
ε: Wall emissivity
σ: Stefan Boltzmann constant = $5.67 * 10^{-8}$, $\mathrm{W/m^2 k^4}$.

Subscripts

c: A Cu-Ag-Hg front contact
e: Exit
f: Fluid
s: Solid
w: Wall of the channel
∞: Ambient or inlet
1: Duct wall at $Y = 0$
2: Duct wall at $Y = 1$.

Conflict of Interests

The authors declare that there is no conflict of interests regarding the publication of this paper.

Acknowledgment

This work was supported by King Abdulaziz City for Science and Technology in Saudi Arabia.

References

[1] C. Min, C. Nuofu, Y. Xiaoli, W. Yu, B. Yiming, and Z. Xingwang, "Thermal analysis and test for single concentrator solar cells," *Journal of Semiconductors*, vol. 30, no. 4, Article ID 044011, 2009.

[2] H. Cotal and J. Frost, "Heat transfer modeling of concentrator multijunction solar cell assemblies using finite difference techniques," in *Proceedings of the 35th IEEE Photovoltaic Specialists Conference (PVSC '10)*, pp. 213–218, Honolulu, Hawaii, USA, June 2010.

[3] D. Vincenzi, F. Bizzi, M. Stefancich et al., "Micromachined silicon heat exchanger for water cooling of concentrator solar cell," in *Proceedings of the PV in Europe Conference and Exhibition—From PV technology to Energy Solutions Conference Record*, pp. 7–11, Rome, Italy, 2002.

[4] B. Moshfegh and M. Sandberg, "Flow and heat transfer in the air gap behind photovoltaic panels," *Renewable and Sustainable Energy Reviews*, vol. 2, no. 3, pp. 287–301, 1998.

[5] A. K. Bhargava, H. P. Garg, and R. K. Agarwal, "Study of a hybrid solar system-solar air heater combined with solar cells," *Energy Conversion and Management*, vol. 31, no. 5, pp. 471–479, 1991.

[6] H. P. Garg and R. S. Adhikari, "Conventional hybrid photovoltaic/thermal (PV/T) air heating collectors: steady-state simulation," *Renewable Energy*, vol. 11, no. 3, pp. 363–385, 1997.

[7] A. A. Hegazy, "Comparative study of the performances of four photovoltaic/thermal solar air collectors," *Energy Conversion and Management*, vol. 41, no. 8, pp. 861–881, 2000.

[8] F. Al-Amri and T. K. Mallick, "Alleviating operating temperature of high concentration solar cell by active cooling," World Renewable Energy Forum, ASES, Denver, Colo, USA, 2012.

[9] F. Al-Amri and T. K. Mallick, "Alleviating operating temperature of concentration solar cell by air active cooling and surface radiation," *Applied Thermal Engineering*, vol. 59, no. 1-2, pp. 348–354, 2013.

[10] H. G. Teo, P. S. Lee, and M. N. A. Hawlader, "An active cooling system for photovoltaic modules," *Applied Energy*, vol. 90, no. 1, pp. 309–315, 2012.

[11] N. S. Kumar, K. Matty, E. Rita et al., "Experimental validation of a heat transfer model for concentrating photovoltaic system," *Applied Thermal Engineering*, vol. 33-34, no. 1, pp. 175–182, 2012.

[12] H. Baig, K. C. Heasman, and T. K. Mallick, "Non-uniform illumination in concentrating solar cells," *Renewable and Sustainable Energy Reviews*, vol. 16, no. 8, pp. 5890–5909, 2012.

[13] A. Royne, C. J. Dey, and D. R. Mills, "Cooling of photovoltaic cells under concentrated illumination: a critical review," *Solar Energy Materials and Solar Cells*, vol. 86, no. 4, pp. 451–483, 2005.

[14] D. B. Tuckerman and R. F. W. Pease, "High-performance heat sinking for VLSI," *Electron Device Letters*, vol. 2, no. 5, pp. 126–129, 1981.

[15] T. M. Harms, M. J. Kazmierczak, and F. M. Gerner, "Developing convective heat transfer in deep rectangular microchannels," *International Journal of Heat and Fluid Flow*, vol. 20, no. 2, pp. 149–157, 1999.

[16] W. Owhaib and B. Palm, "Experimental investigation of single-phase convective heat transfer in circular microchannels," *Experimental Thermal and Fluid Science*, vol. 28, no. 2-3, pp. 105–110, 2004.

[17] J. Y. Min, S. P. Jang, and S. J. Kim, "Effect of tip clearance on the cooling performance of a microchannel heat sink," *International Journal of Heat and Mass Transfer*, vol. 47, no. 5, pp. 1099–1103, 2004.

[18] W. Qu and I. Mudawar, "Experimental and numerical study of pressure drop and heat transfer in a single-phase micro-channel heat sink," *International Journal of Heat and Mass Transfer*, vol. 45, no. 12, pp. 2549–2565, 2002.

[19] L. Micheli, N. Sarmah, X. Luo, K. S. Reddy, and T. K. Mallick, "Opportunities and challenges in micro- and nano-technologies for concentrating photovoltaic cooling: a review," *Renewable and Sustainable Energy Reviews*, vol. 20, pp. 595–610, 2013.

[20] E. Franklin and J. Conventry, "Effect of highly non-uniform illumination distribution on electrical performance of solar cell," in *Proceedings of Solar, Australian and New Zealand Solar Energy Society*, 2003.

[21] J. Coventry, E. Franklin, and A. Blakers, "Thermal and electrical performance of a concentrating PV/thermal collectors: result from ANU CHAPS collector".

[22] J.-L. Domenech-Garret, "Cell behaviour under different non-uniform temperature and radiation combined profiles using a two dimensional finite element model," *Solar Energy*, vol. 85, no. 2, pp. 256–264, 2011.

[23] D. Chemisana and J. I. Rosell, "Electrical performance increase of concentrator solar cells under Gaussian temperature profiles," *Progress in Photovoltaics: Research and Applications*, vol. 21, no. 4, pp. 444–455, 2013.

[24] F. G. Al-Amri and M. A. I. El-Shaarawi, "Combined forced convection and surface radiation between two parallel plates," *International Journal of Numerical Methods for Heat and Fluid Flow*, vol. 20, no. 2, pp. 218–239, 2010.

[25] F. G. Al-Amri and M. A. I. El-Shaarawi, "Mixed convection with surface radiation between two asymmetrically heated vertical parallel plates," *International Journal of Thermal Sciences*, vol. 58, pp. 70–78, 2012.

[26] D. Meneses-Rodríguez, P. P. Horley, J. González-Hernández, Y. V. Vorobiev, and P. N. Gorley, "Photovoltaic solar cells performance at elevated temperatures," *Solar Energy*, vol. 78, no. 2, pp. 243–250, 2005.